HHS Public Access

Author manuscript

J Magn Reson Imaging. Author manuscript; available in PMC 2021 November 03.

Published in final edited form as:

J Magn Reson Imaging. 2020 May ; 51(5): 1369–1381. doi:10.1002/jmri.26949.

Pattern Recognition Analysis of Dynamic Susceptibility Contrast (DSC)-MRI Curves Automatically Segments Tissue Areas With Intact Blood-Brain Barrier in a Rat Stroke Model: A Feasibility and Comparison Study

Seokha Jin, BS[1], **SoHyun Han, PhD**[2], **Radka Stoyanova, PhD**[3], **Ellen Ackerstaff, PhD**[4], **HyungJoon Cho, PhD**[1,*]

[1]Department of Biomedical Engineering, Ulsan National Institute of Science and Technology, Ulsan, South Korea

[2]Center of Neuroscience Imaging Research, Sungkyunkwan University Suwon, South Korea

[3]Department of Radiation Oncology, Miller School of Medicine, University of Miami, Miami, Florida, USA

[4]Department of Medical Physics, Memorial Sloan Kettering Cancer Center, New York, New York, USA

Abstract

Background: The manual segmentation of intact blood-brain barrier (BBB) regions in the stroke brain is cumbersome, due to the coexistence of infarction, large blood vessels, ventricles, and intact BBB regions, specifically in areas with weak signal enhancement following contrast agent injection.

Hypothesis: That from dynamic susceptibility contrast (DSC)-MRI alone, without user intervention, regions of weak BBB damage can be segmented based on the leakage-related parameter K_2 and the extent of intact BBB regions, needed to estimate K_2 values, determined.

Study Type: Feasibility.

Animal Model: Ten female Sprague-Dawley rats (SD, 200–250g) underwent 1-hour middle carotid artery occlusion (MCAO) and 1-day reperfusion. Two SD rats underwent 1-hour MCAO with 3-day and 5-day reperfusion.

Field Strength/Sequence: 7T; ADC and T_1 maps using diffusion-weighted echo planar imaging (EPI) and relaxation enhancement (RARE) with variable repetition time (TR), respectively. dynamic contrast-enhanced (DCE)-MRI using FLASH. DSC-MRI using gradient-echo EPI.

Assessment: Constrained nonnegative matrix factorization (cNMF) was applied to the dynamic ΔR_2^*-curves of DSC-MRI (<4 min) in a BBB-disrupted rat model. Areas of voxels with intact

*Address reprint requests to: HJ.C., Unist-gil 50 (100 Banyeon-ri), Eonyang-eup, Uljugun, Ulsan Metropolitan City, Republic of Korea 689-798. hjcho@unist.ac.kr.

BBB, classified by automated cNMF analyses, were then used in estimating K_1 and K_2 values, and compared with corresponding values from manually-derived areas.

Statistical Tests: Mean ± standard deviation of ΔT_1-differences between ischemic and healthy areas were displayed with unpaired Student's *t*-tests. Scatterplots were displayed with slopes and intercepts and Pearson's *r* values were evaluated between K_2 maps obtained with automatic (cNMF)- and manually-derived regions of interest (ROIs) of the intact BBB region.

Results: Mildly BBB-damaged areas (indistinguishable from DCE-MRI (10 min) parameters) were automatically segmented. Areas of voxels with intact BBB, classified by automated cNMF, matched closely the corresponding, manually-derived areas when respective areas were used in estimating K_2 maps (Pearson's $r = 0.97$, 12 slices).

Data Conclusion: Automatic segmentation of short DSC-MRI data alone successfully identified areas with intact and compromised BBB in the stroke brain and compared favorably with manual segmentation.

Level of Evidence: 3

Technical Efficacy: Stage 1

DYNAMIC SUSCEPTIBILITY CONTRAST magnetic resonance imaging (DSC-MRI) is a quantitative MRI technique to estimate brain perfusion parameters, such as cerebral blood volume (CBV), cerebral blood flow (CBF), and mean transit time (MTT).[1–3] When gadolinium chelates are used as a contrast agent (CA) for DSC-MRI, CA may extravasate through a leaky blood–brain barrier (BBB) in subjects with cerebrovascular diseases.[4–6] The extravasated CA then alters tissue relaxation times, causing bias in DSC-MRI signal signal–time-curves. Thus, investigations have been successfully undertaken regarding systematic measures to compensate for the leakage effects, particularly for tumor DSC-MRI with conspicuous BBB leakage.[6–8]

While BBB leakage has also been assessed by dynamic contrast-enhanced (DCE)-MRI,[9,10] for certain ischemic strokes with weak BBB leakage the standard CA dose (0.1 mmol/kg) may not be adequate to generate sufficiently early (<10 min) tissue T_1 reduction for signal enhancement that can be used to determine small vessel permeability (K^{trans}, the standard measure of BBB permeability).[11] In such a case, alteration of T_2*-based DSC-MRI signal–time-curves at an elevated CA dose (0.3 mmol/kg) due to shortening T_1 from leaky BBB may provide a more sensitive metric when segmenting regions of weakly damaged BBB within a shorter acquisition time (<4 min). Specifically, when the capacity for an increased CA dose is limited for DCE-MRI, with its stronger transverse relaxations, particularly prominent at high field strengths and its longer acquisition times.[12–14] Thus, we hypothesize that the estimation of the vessel wall leakage index K_2 of CA extravasation[5,6,8,15–18] from DSC-MRI (<4 min) at an elevated dose (0.3 mmol/kg) with an intermediate repetition time (TR) (300 msec) can successfully segment BBB-damaged regions in a stroke model with weak BBB damage.

Methodologically, the standard model of K_1 (blood-volume index) and K_2 (leakage index) determination from DSC-MRI requires an unaltered ΔR_2* curve from a region with intact BBB as a reference input function.[5,6,8,15–17] Therefore, the extent of intact BBB must be

known. For tumors, the model typically defines normal regions as nonenhancing voxels after CA injection. However, this assumption may not be readily applicable in cases of weak BBB damage due to ischemic stroke, in which segmentation of normal regions is cumbersome due to the coexistence of infarction, large vessels, ventricles, and normal regions in the same MR slice without apparent signal enhancement via CA injection. Thus, the automatic segmentation of each region from DSC-MRI signal–time-curves may achieve user-independent and objective determination of K_2 values, avoiding the need for auxiliary MR images (diffusion, T_2, and angiography) for region segmentation in addition to DSC-MRI signal–time-curves.

Nonnegative matrix factorization (NMF), which is an unsupervised pattern recognition (PR) algorithm, is fast and can efficiently classify dynamic signals without user intervention and training data.[19–23] Constrained NMF (cNMF) analysis can iteratively search nonnegative matrices of the basic temporal patterns and corresponding weights, which satisfies the data matrix based on multiplicative update algorithms with certain constraints.[24] Previous constrained NMF-based classification of heterogeneous tumor perfusion from DCE-MRI signals was reportedly effective.[19,20] Thus, PR analysis may enable segmentation of BBB-damaged areas, large blood vessels, ventricles, and normal regions in the stroke brain from DSC-MRI signal–time-curves alone, without additional information.

In this study we focused on the automation of K_2 mapping (leakage index) using the cNMF pattern recognition approach to avoid user-dependent manual region of interest (ROI) selection, which appears to be robust in the detection of BBB leakage for models of stroke with weak BBB damage.

Materials and Methods

Animal Model

All experiments ($n = 12$) were approved by the Institutional Animal Care and Use Committee. The transient middle carotid artery occlusion (tMCAO) group of Sprague–Dawley (SD) rats (200–250 g of SD female rats from Orient Bio [Gyeonggi, Republic of Korea]) underwent 1-hour MCAO surgery with intraluminal monofilament (0.35-mm diameter filament, Doccol, Sharon, MA) with 1-day reperfusion. The BBB disruption level can be controlled based on occlusion/reperfusion times[25,26] for the tMCAO model. For a 1-hour occlusion time, corresponding BBB permeability is reportedly increased until 7-day reperfusion.[26] Rat models of 1-hour MCAO with 1-day reperfusion were then used as the stroke group with weak BBB-damage ($n = 4$) for DSC-MRI studies (0.3 mmol/kg, <4 min).[11] Longitudinal T_1 difference (ΔT_1) maps and DCE-MRI (0.1 mmol/kg, <10 min) experiments were performed with 1-day ($n = 3$), 3-day ($n = 1$), and 5-day (confirmed ex vivo Evans blue staining, $n = 1$) reperfusion animal models to evaluate the level of BBB disruption for direct comparison with DSC-MRI. Additional DCE-MRI experiments at the elevated dose of 0.3 mmol/kg were performed for a 1-day reperfusion model ($n = 2$) to directly compare DSC-MRI with DCE-MRI studies at the same dose. Rats were anesthetized with isoflurane during MRI scans with a 7T MR scanner (Bruker Biospin, Germany). For anesthesia, 1–2% isoflurane in a mixture of O_2/N_2O (3:7) was maintained during MRI scans. The body temperature of rats was maintained near 37°C by circulating warm water. The

breathing rates were maintained at about 40 breath/min. To facilitate the CA injection, a 26G catheter was inserted into the tail vein

MRI

After placement of the rat and shimming across the rat brain, multislice T_2-weighted and diffusion-weighted MR images, as well as T_1 maps, were acquired before DSC- or DCE-MRI with CA injection. After DSC- or DCE-MRI, additional T_1 maps were acquired. All experiments were performed with a 7T MR scanner (Bruker Biospin).

T_2-weighted MR images were obtained by using rapid acquisition with relaxation enhancement (RARE)[27] with the following parameters: TR = 5000 msec, RARE factor = 4, effective echo time (TE) = 30 msec, number of averages (NA) = 2, field of view (FOV) = 30 × 30 mm^2, matrix size = 256 × 256, number of slices (NS) = 20, slice gap (SG) = 0 mm, and slice thickness (ST) = 0.5 mm.

Apparent diffusion coefficient (ADC) maps were acquired by using diffusion-weighted echo planar imaging (EPI)[28] with the following parameters: TR = 5000 msec; number of segments = 4; effective TE = 20 msec; b-values = 200, 400, 600, and 1000 smm^{-2}; NA = 1; FOV = 30 × 30 mm^2; matrix size = 96 × 96; NS = 3; SG = 0.2 mm; and ST = 1 mm. Three ADC maps along the *x*, *y*, and *z* directions were averaged to obtain mean ADC values.

T_1 maps were obtained by using RARE with variable TR (RAREVTR)[29] with the following parameters: TR = 80, 150, 200, 400, 800, 1200, 1600, 2000, 2500, 3000, and 4500 msec; RARE factor = 4; effective TE = 4.58 msec; NA = 1; FOV = 30 × 30 mm^2; matrix size = 96 × 96; NS = 3; SG = 0.2 mm; and ST = 1 mm.

DSC-MRI perfusion maps were acquired by using gradient-echo EPI sequence with the following pulse sequence parameters[5]: TR = 300 msec, effective TE = 17 msec, NA = 1, FOV = 30 × 30 mm^2, matrix size = 96 × 96, NS = 3, SG = 0.2 mm, ST = 1 mm, bandwidth = 3.5 × 10^5 Hz, number of segments = 1, flip angle (FA) = 35°, number of repetitions (NR) = 800, and temporal resolution = 0.3 sec. The dose of the administered CA gadoterate meglumine (Gd-DOTA) was 0.3 $mmol{\cdot}kg^{-1}$ (130 μl). Pre- and post-CA injection acquisition times were 1 and 3 min, respectively.

DCE-MRI data were acquired by using fast low-angle shot (FLASH)[30] with the following parameters: TR = 35 msec, TE = 1.9 msec, NA = 1, FOV = 30 × 30 mm^2, matrix size = 96 × 96, NS = 3, SG = 0.2 mm, ST = 1 mm, FA = 30°, NR = 180, and temporal resolution = 3.36 sec. The Gd-DOTA injection dose for DCE-MRI was 0.1 $mmol{\cdot}kg^{-1}$, followed by a 0.2 $mmol{\cdot}kg^{-1}$ flush 15 min after DCE-MRI acquisition to sequentially obtain ΔT_1 maps and improve contrast. The cumulative injected dose was 0.3 $mmol{\cdot}kg^{-1}$. Pre- and post-CA injection acquisition times were 1 and 9 min, respectively. Additional DCE-MRI experiments ($n = 2$) with the injection dose of 0.3 mmol/kg (same dose as DSC-MRI) were acquired for 20 min.

Ex Vivo Assessment of BBB Breakdown and Extent of Ischemia

Triphenyl tetrazolium chloride (TTC) and Evans blue stain were performed for estimating infarction[31] and BBB disrupted region,[32] respectively. Evans blue leakage in areas of damaged BBB was assessed ex vivo in a 5-day reperfusion model, to validate the association of postinjection T_1 changes and BBB disruption. Post-MRI scans, a 3% Evans blue solution (3 ml/kg of body weight) was injected via the tail vein. After 30 min, the brain was perfused with 4°C saline and axially sectioned with 2-mm thickness. The slices were stained with a 1% TTC solution at 25°C for 10 min to detect the extent of the ischemic lesion by S.H.J. (4 years of experience). To validate the association between BBB-disrupted lesion from Evans blue leakage and ΔT_1 map, respectively, thresholded masks were generated and the Dice coefficient was calculated between them.

Data Analysis

To obtain relative CBV (rCBV) maps, $\Delta R_2^*(t) = -\frac{1}{TE} ln\left(\frac{S(t)}{S_{pre}}\right)$ was converted from the DSC-MRI signal, where S(t) is the DSC-MRI signal and S_{pre} is an averaged preinjection signal in DSC-MRI. By fitting $\Delta R_2^*(t)$ with the gamma variate function, rCBV values were calculated from the area of the fitted curve.[1]

For ADC calculations, each gradient direction of the ADC map was estimated with the following equation: $S = S_0 \times e^{-ADC \times b}$.[28,33] Representative ADC maps were computed by averaging three gradient directions of ADC maps.

Vessel permeabilities were evaluated using an extended Tofts model to obtain K^{trans}, V_e, and V_p maps from DCE-MRI signal–time-curves.[30] The extended Tofts model was applied with the following equation: $C_t(t) = v_p C_p(t) + K^{trans} \int_0^t C_p(t') \exp\left(\frac{K^{trans}(t-t)}{v_e}\right) dt'$, where C_t and C_p represent CA concentration of tissue and blood, respectively. C_p was estimated from the internal carotid artery for each animal.

To confirm CA leakage, the ΔT_1 map was computed by subtracting the postinjection T_1 map from the preinjection T_1 map, with ΔT_1 longitudinally calculated at selected timepoints up to 85 min after CA injection.

To obtain K_1 and K_2 maps from DSC-MRI signal–time-curves, a ΔR_2^* vs. time curve of each voxel was fitted with arrival time and time scaling corrections[16]: $\Delta R_2^*(t) = K_1 \Delta \bar{R}_2^*\left(\frac{t+\tau}{\alpha}\right) - K_2 \int_0^t \Delta \bar{R}_2^*\left(\frac{t'+\tau}{\alpha}\right) dt'$, where $\Delta \bar{R}_2^*$ represents an averaged ΔR_2^* curve for brain tissue regions with intact BBB, α is a time scaling factor, and τ is a time offset. K_1 and K_2 values then reflect cerebral blood volume and CA leakage, respectively. To calculate the $\Delta \bar{R}_2^*$ curve, the ROIs were drawn manually on striatum of contralateral hemisphere by considering the T_2-weighted image, ADC and rCBV maps, and then ΔR_2^* curves within ROIs were averaged.

To automatically segment the tissue region of intact BBB, cNMF was applied to $\Delta R_2^*(t)$ curves generated from DSC-MRI of rat stroke models. Detailed cNMF algorithms were

described in a previous study,[19,20,24] and were largely followed here, except for signal normalization. Briefly, to find nonnegative matrices S and W, representing the basic temporal curves and corresponding weights, respectively, that satisfy modeling of the data matrix $V \approx WS$, multiplicative update algorithms were used. For initialization, W was constructed with random numbers (from 0 to 1) and the constrained (nonnegative) pseudoinversion matrix of W was allocated to initial S. Updates of W and S were performed by multiplicative update algorithms: $\begin{cases} W \leftarrow W\frac{(VS^T)}{(VSS^T)} \\ S \leftarrow S\frac{(W^TV)}{(W^TWV)} \end{cases}$. After each update process of W or S, negative elements in W or S were set to a small positive number ε (=2.2204×10^{-16}, MatLab, R2016b, MathWorks, Natick, MA). This procedure was continued until the iteration error $\left(= \frac{(\delta^{(q)} - \delta^{(q+1)})}{\delta^{(q)}},\ where\ \delta = \parallel V - WS \parallel,\ q\ is\ the\ number\ of\ iteration \right)$ was lower than 10^{-8}. Brain tissue selected within the skull boundary was used for cNMF analysis.

For large-vessel segmentation (high blood volume fraction), cNMF with k (number of the pattern) = 1 was applied to the unnormalized ΔR_2*(t) curves. As the signal of the ΔR_2*(t) curves reflects the blood volume for a healthy brain, the weight of such (k = 1) cNMF represents the blood volume fraction for each voxel. For the validation, the cNMF weights map were compared with the corresponding rCBV and K_1 map. The scatterplot between cNMF weight and K_1 values were plotted within the ROI of a healthy brain region.

Separately, for the segmentation of voxels with intact BBB, cNMF with k = 2 was applied to a normalized ΔR_2*(t) curve. Normalization was performed to minimize blood volume heterogeneity (signal maximum in any specific pixel dependent on CA agent concentration and blood volume) by dividing the decaying stages of ΔR_2*(t) with their maximum values, as shown in Supporting Information Fig. S1. Briefly, the signal of ΔR_2*(t) curves in each voxel is scaled such that the maximum signal is equal to 1 for cNMF pattern recognition for voxels with differential K_2 segmentation, as shown in Supplementary Fig. S1. Then, for k = 2, the cNMF weights difference map was defined by the difference between W matrix values of the first (fast decay) component and the second (slow decay) component from cNMF analyses. For validation, the cNMF weights difference map was compared with the ΔT_1 and K_2 map. The scatterplot between cNMF weights difference and K_2 values were plotted within the ROI of the BBB-damaged region.

Automatic segmentation was then performed based on the cNMF weights (k = 1) and cNMF weights difference map (k = 2) to respectively delineate the region of large vessel and damaged BBB. When the cNMF weights map of k = 1 was larger than 1 (empirically set based on comparison with the corresponding rCBV map), the region was classified as a large vessel region. Regions in which cNMF weights difference maps of k = 2 were larger than 0.1, between 0 and 0.1, and smaller than 0 were defined as BBB-disrupted (or ventricles), mixture, and intact BBB regions, respectively (empirically set based on comparison with the corresponding ΔT_1 map). The validity of these thresholds are shown in Supporting

Information Fig. S2. The ventricles were further segmented based on the arrival time of contrast agent.[34] Finally, the tissue region of intact BBB was then segmented by excluding large-vessel areas (from $k = 1$ cNMF) from intact BBB regions (from $k = 2$ cNMF).

To compare enhancement patterns of ΔR_2^* curves or decay patterns of normalized ΔR_2^* curves according to different tissue types, for short DSC-MRI acquisition (<4 min) with an elevated CA dose (0.3 mmol/kg), five different ROIs (sinus, ventricle, infarction, contralateral cortex, contralateral striatum) were drawn based on the T_2-weighted image, and ADC and rCBV maps. Each ROI, depicting a representative region for each tissue type, was chosen to be 3 × 3 voxels, to keep the ROI the same size for the different tissue types, including the distinct anatomical structures of smaller size, such as ventricles and sinus.

To study the effects of ROI segmentation of the tissue region of intact BBB regions on the determination of K_2 or K_1 maps, five different ROIs (infarctions from diffusion map, ventricles from T_2-weighted MR image, large vessels from blood volume map, manual ROI of intact BBB region, and automatic ROI of intact tissue region from cNMF analyses) were used as $\Delta \overline{R}_2^*$. To show how important the choice of the tissue region of intact BBB, respective K_1 and K_2 maps were compared among the ROIs. K_1 and K_2 maps derived from manual ROIs of the tissue region of intact BBB in the contralateral striatum area, which were collectively selected from diffusion maps, T_2-weighted MR images and angiograms were considered as reference values for the direct comparisons with the rest.

To study the effects of the acquisition time of DSC-MRI on cNMF analysis, perfusion parameters (K_1, K_2, cNMF weight with $k = 1$ and cNMF weight difference with $k = 2$) were computed with the intentionally limited number of data (the number of used data corresponded to the following acquisition times: 0.5, 1, 1.5, 2, 2.5, 2.85 min). The K_1 and K_2 map with a manually drawn ROI of a healthy brain region are compared with cNMF weights and cNMF weights difference maps.

Statistical Analysis

To verify K^{trans} and V_e differences between ischemic and healthy areas, and also to validate the association between ΔT_1 differences and K_2 values from cNMF segmented lesions of BBB damage and healthy areas, the mean and standard deviation (SD) of corresponding values were displayed and accompanying significance analyses were run with unpaired Student's *t*-tests with a significance level of 0.05 using MatLab. To validate the linearity of K_1 and K_2 maps obtained with the automatic ROI of the intact BBB region from cNMF analyses with respect to the reference maps, scatterplots were displayed with slopes and intercepts and Pearson's *r* values were evaluated.

MCAO occlusion/reperfusion times, MRI acquisitions, and the number of animals used are summarized in Table 1.

Results

As shown in Fig. 1a, lesions with reduced ADC values were observed, but there were no noticeable changes in the 0.1 mmol/kg-injected ΔT_1 maps (Fig. 1a, post-10 min CA

injection). However, there were increases of ΔT_1 on the ipsilateral hemisphere in the 0.3 mmol/kg-injected (cumulative) ΔT_1 map (Fig. 1a, post-55 min CA injection). For direct comparisons, corresponding maps were generated for the 1-hour MCAO with 3-day and 5-day reperfusion after surgery, respectively, where increases of ΔT_1 were observed in the ipsilateral brain at 10 min post-0.1 mmol/kg CA injection (Fig. 1b,c). The hyperintensity area on the ΔT_1 map (>850 msec) in the ipsilateral lesion colocalized (Dice coefficient = 0.8825) with the corresponding Evans blue staining (Fig. 1c, 4th column), validating the use of ΔT_1 values as standard BBB leakage index for the 1-hour MCAO reperfusion model. Longitudinal ΔT_1 values were compared between the infarct and the normal area for the 1-day and 3-day reperfusion model in Fig. 1d. As shown for control experiments, no increase of ΔT_1 in the ipsilateral lesions was observed for 1-hour MCAO with 1-day reperfusion without CA injection. The differences in ΔT_1 values between the infarct and the healthy areas are plotted in Fig. 1e,f for 0.1 mmol/kg (10 min post-CA injection) and 0.3 mmol/kg injection (55 min post-CA injection), respectively. The 1-hour MCAO with 1-day reperfusion models exhibit negligible ΔT_1 changes ($P = 0.887$) within 10 min post-0.1 mmol/kg CA injection. An elevated CA dose of 0.3 mmol/kg was required to increase ΔT_1 changes ($P = 0.035$), highlighting the weak BBB damage of the 1-day reperfusion model compared with the 3-day and 5-day reperfusion models.

Injecting a higher 0.3 mmol/kg CA dose (equivalent to the dose of the DSC-MRI experiments) in one injection did not improve the detectability of subtle BBB damage in the first 10 min post-CA injection of the DCE-MRI in the 1-hour MCAO with 1-day reperfusion model (Fig. 2a,b). In both CA injection dose regimens (0.1 mmol/kg followed by 0.2 mmol/kg flush or 1 × 0.3 mmol/kg), ΔT_1 (or ΔR_1) values differed between infarcted and healthy brain regions only later (post-55 min of CA injection) in the DCE-MRI for the 1-day reperfusion model (Figs. 1, 2), with a clear deviation of ΔR_1 curves between the ipsilateral infarcted and contralateral healthy brain being observed only after ~10 min or more of DCE-MRI acquisition (Figs. 1d, 2e). These late curve detectable ΔT_1 (or ΔR_1) differences did not translate into noticeable differences ($P = 0.631$, 0.583, respectively) in the K^{trans} and V_e values (Fig. 2h). Using a 1-hour MCAO rat with 3-day reperfusion model, the modest or not observable CA leakage and ΔT_1 (or ΔR_1) differences become detectable at early times post-CA injection by DCE-MRI, as represented by the higher K^{trans}, V_e, and V_p in the infarction than the contralateral healthy brain (Fig. 2c,g,h). These data confirm the previously observed[11,26] difficulties in segmenting subtle BBB-damage with a short DCE-MRI (<10 min) acquisition at both CA doses of 0.1 mmol/kg and 0.3 mmol/kg.

Five different ROIs (sinus, ventricle, infarction, contralateral cortex, contralateral striatum, colored arrows in Fig. 3a) were marked on the T_2-weighted image (Fig. 3a), based on ADC (Fig. 3b) and rCBV (Fig. 3c) maps. Raw ΔR_2* graphs in Fig. 3d showed that sinus and ventricle regions exhibited the largest and smallest peak enhancements among the five ROIs, respectively. For normalized ΔR_2* curves, ventricle and infarction regions exhibited the fastest signal decays, while the sinus showed the slowest signal decay when compared with signals of the contralateral normal cortex and striatum regions (Fig. 3e).

Figure 4 shows the cNMF with $k = 1$ results for large vessel segmentation. As shown in Fig. 4a–c, the cNMF weights map exhibited similar contrast on both the rCBV and K_1 maps.

When cNMF weights values were larger than 1, the voxels were then assigned to the large vessel region (marked as red color in Fig. 4d). A representative curve from cNMF ($k = 1$) is shown in Fig. 4e. For all cases, cNMF weight values related strongly to K_1 values (Fig. 4f, Pearson's $r = 0.9884$, 0.9913, 0.9830, and 0.9794). A linear but not identical correlation is assumed for the relationship between cNMF weight ($k = 1$) and K_1, as both values were calculated based on different relative scales.

Figure 5 shows the cNMF with $k = 2$ results for ventricle and BBB-disrupted region segmentation. Infarction and BBB-disrupted regions were detected by ADC mapping (Fig. 5a) and ΔT_1 mapping (55 min post-0.3 mmol/kg CA injection for DSC-MRI, Fig. 5b), respectively. The cNMF weights difference map and K_2 map exhibited similar contrast, as shown in Fig. 5c,d. Figure 5e shows the segmentation results of BBB-disrupted (red), mixture (green), and intact BBB (blue) regions. Representative cNMF curves of fast-decay (first) and slow-decay (second) components are shown in Fig. 5f. The K_2 and cNMF weights difference correlated strongly, as shown in Fig. 5g (Pearson's $r = 0.9071$, 0.8401, 0.9478, and 0.8452). Again, a linear but not identical correlation was expected between cNMF weights difference ($k = 2$) and K_2, as both values are calculated based on different relative scales. Red colored regions from the automatic cNMF segmentation primarily coincided with regions of BBB damage ($\Delta T_1 > 250$ msec) from the corresponding ΔT_1 map in the same row. Conversely, regions from ΔT_1 maps generally encompassed larger areas in the ipsilateral brain than areas from the cNMF segmentations, except for ventricle areas selected by cNMF segmentations. The automated segmentation (yellow: ventricle, red: BBB-damaged regions, green: a mixture of healthy and BBB-damaged brain, blue: healthy brain, gray: large vessels) of a representative slice are shown enlarged in Fig. 5h. The values of ΔT_1 from cNMF classified BBB-damaged regions (red) were significantly different ($P = 0.020$) from those of corresponding normal tissue, as shown in Fig. 5i, indicating the association of BBB-damage with DSC-MRI derived leakage index (K_2).

As shown in Fig. 6a–g, five different ROIs (infarction (blue), ventricle (orange), large vessel (green), manual-ROI (red), automated cNMF-ROI (yellow)) were overlaid on the anatomical MR image. For all cases, K_1 maps exhibited similar contrast to each other, regardless of variations in ROI. As shown in Fig. 6h, all K_1 maps related strongly to manually drawn ROIs (Pearson's $r = 0.9862$, 0.9978, 0.9982, and 0.9989). Additionally, correlation coefficients between K_1 from manual ROIs and automatic cNMF ROIs were > 0.99 for all rats (Fig. 6i, Pearson's $r = 0.9987$, 0.9989, 0.9950, and 0.9957).

However, when infarction and ventricle regions were considered as intact BBB regions, the corresponding K_2 values in infarction lesion were underestimated in comparison to K_2 values derived from manual ROI, as shown in Fig. 7c,d. Scatterplots between K_2 values derived from various ROIs and manual ROIs showed that the values derived from infarction and ventricle regions exhibited lower correlation (blue and orange color in Fig. 7h, Pearson's $r = 0.6976$ and 0.4409, respectively). When large vessel regions were selected as healthy brain regions in the fitting, as shown in Fig. 7e, the Pearson's r was 0.8046, slightly lower than that of the automatic ROI (black color in Fig. 7h, Pearson's $r = 0.9117$). Automated cNMF ROI-derived K_2 values (Fig. 7f) were highly correlated with respect to manual ROI

(Fig. 7g) for all rats (12 slices from four rats), as plotted in Fig. 7i (Pearson's r = 0.9997, 0.9117, 0.9761, and 0.9813).

The scan-time durations for fitting and PR analysis influenced the estimation of perfusion parameters (K_1, K_2) and cNMF weights, as shown in Supporting Information Figs. S3 and S4, respectively. K_1 and cNMF weight maps were relatively robust to changes of acquisition times post-CA injection, as shown in Supporting Information Fig. S3a,b. K_1 values ($K_{1,\ 0.5\ min}$), which were fitted from data within 0.5-min postinjection, correlated highly to the full data ($K_{1,\ 2.85\ min}$, Pearson's r = 0.9765). For cNMF weights ($cNMF_{0.5\ min,\ k\ =\ 1}$), the Pearson's r value with $cNMF_{2.85\ min}$ was 0.9733. This trend was consistent for other animals, as shown in Supporting Information Fig. S3c,d. However, K_2 values were highly sensitive to the length of the acquisition. The $K_{2,\ 0.5\ min}$ map showed little permeability-oriented contrast. Permeability contrast became consistent for acquisition times over 2 min, as shown in Supporting Information Fig. S4a. Similar behavior was observed for the maps of the cNMF weights, as shown in Supporting Information Fig. S4b. The Pearson's r values for $K_{2,\ 0.5\ min}$ with $K_{2,\ 2.85\ min}$ and $cNMF_{0.5\ min,\ k\ =\ 2}$ with $cNMF_{2.85\ min,\ k\ =\ 2}$ were 0.3147 and 0.1259, respectively (Supporting Information Fig. S4c,d). The Pearson's r values for $K_{2,\ 2\ min}$ with $K_{2,\ 2.85\ min}$ and $cNMF_{2\ min,\ k\ =\ 2}$ with $cNMF_{2.85\ min,\ k\ =\ 2}$ were 0.9488 and 0.9636, respectively. This trend was consistent for other rats, as shown in Supporting Information Fig. S4c,d. Subsequently, cNMF analysis of DSC-MRI did not require a longer scan time than necessary for regular model-based fitting. At least 2 min acquisition of DSC-MRI is required both for K_2 fitting and cNMF analysis to obtain BBB-leakage related contrast in this reperfusion model.

As shown in Supporting Information Fig. S5 for certain cases, the hyperintensity area on ΔT_1 maps is markedly larger and encompasses the region with elevated K_2 values of DSC-MRI. Furthermore, the regions with higher ΔT_1 (red area in the second column) are generally observed to coincide with regions exhibiting elevated K_2 (red area in the third column).

Discussion

Although the K_1, K_2 model of DSC-MRI is widely used to measure true CBV (K_1 index) without CA extravasation effects,[6,8,17,35] numerous studies also attempted to evaluate vascular permeability (K_2 index) of neurovascular disease,[5,6,8,15–18] which requires the robust delineation of tissue region of intact BBB. Often, nonenhancing voxels with CA injection were selected to obtain $\Delta\bar{R}_2^*$ curves of intact BBB from DSC-MRI,[6] because vessel permeability information cannot be obtained from anatomical/structural images. However, for brain tissue with mild BBB-damaged lesions, such as the 1-hour MCAO 24-h reperfusion model, it turns out to be difficult to objectively segment tissue regions of intact BBB even with short DCE-MRI acquisition. Consequently, incorrectly chosen $\Delta\bar{R}_2^*$ curves are observed to deteriorate the following K_2 estimation. Namely, K_2 values were observed to be sensitive to both ROI selection for $\Delta\bar{R}_2^*$ curve and scan-time durations. Thus, an automatic pattern recognition method would facilitate the robust segmentation of the

tissue region of intact BBB, and cNMF-based segmentation is observed to be effective for distinguishing the region of mild BBB-leakage from DSC-MRI.

On the other hand, our results also manifest the underlying difficulties of absolute intersubject comparisons of conventional K_2 values of DSC-MRI. The issues mainly come from different patterns of $\Delta\bar{R}_2^*$ curve between subjects. Several factors, such as CA injection speed, the physiological condition of a subject, and resulting heterogeneity of ΔR_2* patterns even in healthy tissue may affect the shape of $\Delta\bar{R}_2^*$ curve from intact BBB. Therefore, as shown from varying intercepts of scatterplots between automatic- and manual (striatum)-ROI derived K_2 values among different rats, the user-independent voxel selections of intact BBB regions may be a more objective procedure when intersubject comparisons are necessary, especially when the location of the lesion is unknown a priori.

It was also worthwhile to compare the sensitivity of various MR protocols in detecting mild BBB damage. A dose of 0.3 mmol/kg Gd-DOTA was chosen for the DSC-MRI in this study to obtain a good contrast-to-noise ratio, as commonly used in preclinical applications.[36–39] While 0.1 mmol/kg CA is a typical dose for most preclinical DCE-MRI studies, in our study K_2 from DSC-MRI (<4 min) appeared to be more sensitive to the BBB-damaged region than K^{trans} from DCE-MRI (<10 min), even with the same CA dose. High temporal resolution (0.3 sec) with good signal contrast of ΔR_2* curves from the elevated injection dose appears to be advantageous in detecting BBB-leakage related blood volume alterations of DSC-MRI in a relatively short acquisition time (<4 min). On the other hand, due to the leakage of CA, there is the possibility of complementary T_2*-lengthening, as the susceptibility difference between blood vessel and tissue areas may be reduced. The extent of T_2*-lengthening and the effect on the DSC-MRI time curve due to CA leakage should be explored, as it would reduce ΔR_2*-contrast in the same manner as the shortening of T_1.

Within the scope of this study, the overlap of elevated K_2 and large ΔT_1 regions warrants the validity of K_2 as a vessel wall leakage index, as the difference in T_1 values before and after (55 min) CA injection at the dose of 0.3 mmol/kg of reperfused brain should clearly indicate the region with leaking BBB as validated by representative Evans Blue staining results. As a control, there was no increase of ΔT_1 in ipsilateral lesions without any CA injection for the corresponding model as well during the time-courses of MRI experiments. However, caution should be exercised when making direct one-to-one comparisons and interpretations between with ΔT_1 and K_2 values from DSC-MRI. Variations of CA concentration in imaging voxels due to differing perfusion and diffusion times of CA after injection (55 min for ΔT_1, 2–3 min for DSC-MRI) may confound the direct comparisons.

Limitations of this study are as follows. First, because it has been reported that preinjection of CA before DSC-MRI acquisition significantly reduces leakage-oriented DSC-MRI signal alterations,[11] longitudinal studies between DCE-MRI and DSC-MRI were not pursued in the same animal model. The availability of simultaneous DCE- and DSC-MRI acquisitions at an elevated dose (~0.3 mmol/kg) may provide more direct comparisons between DCE- and DSC-MRI signal–time-curves. Second, we measured absolute T_1 values before and after CA injection, which would shorten if CA leaked into the interstitial space through

BBB openings of similar size. Notably, ΔT_1 changes involve confounding factors, such as blood volume, interstitial space, and CA diffusion characteristics other than vessel wall permeability. Thus, direct comparisons between histology and in vivo MRI require caution, beyond issues related to in vivo – ex vivo alignment and vastly different imaging volumes. Third, when comparing the sensitivity of K^{trans} and K_2, the larger number of animals for various occlusion/reperfusion times of the MCAO model should be further investigated. In this study, we focused on the automation of K_2 mapping for the 1-hour MCAO 24-hour reperfusion model, which has mild BBB-damage.

In conclusion, cNMF-based pattern recognition analysis was applied to dynamic ΔR_2* curves of DSC-MRI (<4 min) for a rat model of 1-hour MCAO with 1-day reperfusion demonstrating weak BBB disruption. Pixels were automatically segmented as BBB-damaged, ventricles, large blood vessels, and normal tissue regions from signal–time-curves of DSC-MRI. By comparing K_1 and K_2 parameters derived from automatic (classified from cNMF-based segmentation of DSC-MRI alone) and manual (selected from T_2-weighted images, ADC maps, and CBV maps) ROIs of intact BBB region, the usefulness of cNMF-based segmentation for the automation of voxel selections with differential vessel wall leakage index (K_2) was demonstrated, particularly in evaluating DSC-MRI parameters for a stroke model with weak BBB damage. Clinically, this type of analysis might improve the observer-independent assessment of the stroke area, especially at early timepoints of stroke occurrence, where DCE-MRI has limited detectability.[40]

Supplementary Material

Refer to Web version on PubMed Central for supplementary material.

Acknowledgments

Contract grant sponsor: National Research Foundation of Korea (NRF); Contract grant sponsor: Korean government; Contract grant numbers: 2018M3C7A1056887 and 2018R1A6A1A03025810; Contract grant sponsor: Memorial Sloan-Kettering Cancer Support; Contract grant number: P30 CA008748.

References

1. Calamante F, Thomas DL, Pell GS, Wiersma J, Turner R. Measuring cerebral blood flow using magnetic resonance imaging techniques. J Cereb Blood Flow Metab 1999;19:701–735. [PubMed: 10413026]
2. Cha S, Knopp EA, Johnson G, Wetzel SG, Litt AW, Zagzag D. Intracranial mass lesions: Dynamic contrast-enhanced susceptibility-weighted echo-planar perfusion MR imaging. Radiology 2002;223:11–29. [PubMed: 11930044]
3. Zierler KL. Theoretical basis of indicator-dilution methods for measuring flow and volume. Circ Res 1962;10:393–407.
4. Bang OY, Saver JL, Alger JR, et al. Patterns and predictors of blood-brain barrier permeability derangements in acute ischemic stroke. Stroke 2009;40:454–461 [PubMed: 19038915]
5. Haselhorst R, Kappos L, Bilecen D, et al. Dynamic susceptibility contrast MR imaging of plaque development in multiple sclerosis: Application of an extended blood-brain barrier leakage correction. J Magn Reson Imaging 2000;11:495–505 [PubMed: 10813859]
6. Boxerman JL, Schmainda KM, Weisskoff RM. Relative cerebral blood-volume maps corrected for contrast agent extravasation significantly correlate with glioma tumor grade, whereas uncorrected maps do not. Am J Neuroradiol 2006;27:859–867. [PubMed: 16611779]

7. Dósa E, Guillaume DJ, Haluska M, et al. Magnetic resonance imaging of intracranial tumors: Intra-patient comparison of gadoteridol and ferumoxytol. Neurooncology 2010;13:251–260.
8. Quarles CC, Ward BD, Schmainda KM. Improving the reliability of obtaining tumor hemodynamic parameters in the presence of contrast agent extravasation. Magn Reson Med 2005;53:1307–1316. [PubMed: 15906288]
9. Heye AK, Thrippleton MJ, Armitage PA, et al. Tracer kinetic modeling for DCE-MRI quantification of subtle blood-brain barrier permeability. Neuroimage 2016;125:446–455. [PubMed: 26477653]
10. Villringer K, Sanz Cuesta BE, Ostwaldt A-C, et al. DCE-MRI blood-brain barrier assessment in acute ischemic stroke. Neurology 2017;88: 433–440. [PubMed: 28031392]
11. Jin SH, Kang MS, Cho H. Cerebral blood perfusion deficits by dynamic susceptibility contrast (DSC)-MRI with gadolinium chelates in rats with postischemic reperfusion without significant dynamic contrast enhanced (DCE)-MRI derived vessel permeabilities: A cautionary note. Plos One 2018;13:e0201076.
12. Heilmann M, Walczak C, Vautier J, et al. Simultaneous dynamic T_1 and T_2* measurement for AIF assessment combined with DCE MRI in a mouse tumor model. Magn Reson Mater Phys Biol Med 2007;20: 193–203.
13. Fruytier AC, Magat J, Colliez F, et al. Dynamic contrast-enhanced MRI in mice at high field: Estimation of the arterial input function can be achieved by phase imaging. Magn Reson Med 2014;71:544–550. [PubMed: 23440927]
14. Han S, Cho H. Temporal resolution improvement of calibration-free dynamic contrast-enhanced MRI with compressed sensing optimized turbo spin echo: The effects of replacing turbo factor with compressed sensing accelerations. J Magn Reson Imaging 2016;44:138–147. [PubMed: 26713414]
15. Taoka T, Kawai H, Nakane T, et al. Application of histogram analysis for the evaluation of vascular permeability in glioma by the K2 parameter obtained with the dynamic susceptibility contrast method: Comparisons with Ktrans obtained with the dynamic contrast enhance method and cerebral blood volume. Magn Reson Imaging 2016;34.7:896–901. [PubMed: 27109485]
16. Leigh R, Jen SS, Varma DD, Hillis AE, Barker PB. Arrival time correction for dynamic susceptibility contrast MR permeability imaging in stroke patients. PLoS One 2012;7:e52656.
17. Donahue KM, Krouwer HG, Rand SD, et al. Utility of simultaneously acquired gradient-echo and spin-echo cerebral blood volume and morphology maps in brain tumor patients. Magn Reson Med 2000;43: 845–853. [PubMed: 10861879]
18. Bonekamp D, Deike K, Wiestler B, et al. Association of overall survival in patients with newly diagnosed glioblastoma with contrast-enhanced perfusion MRI: Comparison of intraindividually matched T_1-and T_2*-based bolus techniques. J Magn Reson Imaging 2015;42:87–96. [PubMed: 25244574]
19. Stoyanova R, Huang K, Sandler K, et al. Mapping tumor hypoxia in vivo using pattern recognition of dynamic contrast-enhanced MRI data. Transl Oncol 2012;5:437–447. [PubMed: 23326621]
20. Han S, Stoyanova R, Lee H, et al. Automation of pattern recognition analysis of dynamic contrast-enhanced MRI data to characterize intratumoral vascular heterogeneity. Magn Reson Med 2018;79: 1736–1744. [PubMed: 28727185]
21. Chang YCC, Ackerstaff E, Tschudi Y, et al. Delineation of tumor habitats based on dynamic contrast enhanced MRI. Sci Rep 2017;7:9746. [PubMed: 28851989]
22. Lee JS, Lee DD, Choi S, Park KS, Lee DS. Non-negative matrix factorization of dynamic images in nuclear medicine. Nuclear Science Symposium Conference Record, 2001 IEEE. 2001;4:2027–2030.
23. Wang D, Xiao M, Zhang Y, Wan M. Abdominal parametric perfusion imaging with respiratory motion-compensation based on contrast-enhanced ultrasound: In-vivo validation. Comput Med Imaging Graph 2018;65:11–21. [PubMed: 28666563]
24. Sajda P, Du S, Brown TR, et al. Nonnegative matrix factorization for rapid recovery of constituent spectra in magnetic resonance chemical shift imaging of the brain. IEEE Trans Med Imaging 2004;23: 1453–1465. [PubMed: 15575404]

25. Neumann-Haefelin T, Kastrup A, de Crespigny A, et al. Serial MRI after transient focal cerebral ischemia in rats: Dynamics of tissue injury, blood-brain barrier damage, and edema formation. Stroke 2000;31: 1965–1972. [PubMed: 10926965]
26. Lin CY, Chang C, Cheung WM, et al. Dynamic changes in vascular permeability, cerebral blood volume, vascular density, and size after transient focal cerebral ischemia in rats: Evaluation with contrast-enhanced magnetic resonance imaging. J Cereb Blood Flow Metab 2008;28: 1491–1501. [PubMed: 18478021]
27. Hennig J, Nauerth A, Friedburg H. RARE imaging: A fast imaging method for clinical MR. Magn Reson Med 1986;3:823–833. [PubMed: 3821461]
28. Meng X, Fisher M, Shen Q, et al. Characterizing the diffusion/perfusion mismatch in experimental focal cerebral ischemia. Ann Neurol 2004;55: 207–212. [PubMed: 14755724]
29. Lee DK, Han SH, Cho H. Optimization of sparse phase encodings for variable-repetition-delay turbo-spin echo (TSE) T1 measurements for preclinical applications. J Magn Reson 2017;274:57–64. [PubMed: 27886558]
30. Roberts C, Issa B, Stone A, et al. Comparative study into the robustness of compartmental modeling and model-free analysis in DCE-MRI studies. J Magn Reson Imaging 2006;23:554–563. [PubMed: 16506143]
31. Busch E, Krüger K, Hossmann K-A. Improved model of thromboembolic stroke and rt-PA induced reperfusion in the rat. Brain Res 1997; 778:16–24. [PubMed: 9462873]
32. Uyama O, Okamura N, Yanase M, et al. Quantitative evaluation of vascular permeability in the gerbil brain after transient ischemia using Evans blue fluorescence. J Cereb Blood Flow Metab 1988;8:282–284. [PubMed: 3343300]
33. Stejskal EO, Tanner JE. Spin diffusion measurements: Spin echoes in the presence of a time-dependent field gradient. J Chem Phys 1965; 42:288–292.
34. Kao YH, Guo WY, Wu YT, et al. Hemodynamic segmentation of MR brain perfusion images using independent component analysis, thresholding, and Bayesian estimation. Magn Reson Med 2003;49: 885–894. [PubMed: 12704771]
35. Boxerman JL, Prah DE, Paulson ES, et al. The role of preload and leakage correction in gadolinium-based cerebral blood volume estimation determined by comparison with MION as a criterion standard. Am J Neuroradiol 2012;33:1081–1087. [PubMed: 22322605]
36. Wirestam R, Ryding E, Lindgren A, et al. Absolute cerebral blood flow measured by dynamic susceptibility contrast MRI: A direct comparison with Xe-133 SPECT. Magma 2000;11:96–103. [PubMed: 11154950]
37. Chen F, Feng Y, Zheng K, et al. Enhanced antitumor efficacy of a vascular disrupting agent combined with an antiangiogenic in a rat liver tumor model evaluated by multiparametric MRI. PLoS One 2012;7: e41140.
38. Mystkowska D, Tutas A, Jezierska-Wozniak K, et al. Usefulness of clinical magnetic resonance scanners for imaging experimental changes in laboratory rodents' central nervous system. Polish Ann Med 2012;19: 43–49.
39. Chyi T, Chang C. Temporal evolution of 3-nitropropionic acid-induced neurodegeneration in the rat brain by T2-weighted, diffusion-weighted, and perfusion magnetic resonance imaging. Neuroscience 1999;92: 1035–1041. [PubMed: 10426543]
40. Welker K, Boxerman J, Kalnin XA, et al. ASFNR recommendations for clinical performance of MR dynamic susceptibility contrast perfusion imaging of the brain. Ame J Neuroradiol 2015;36:E41–E51.

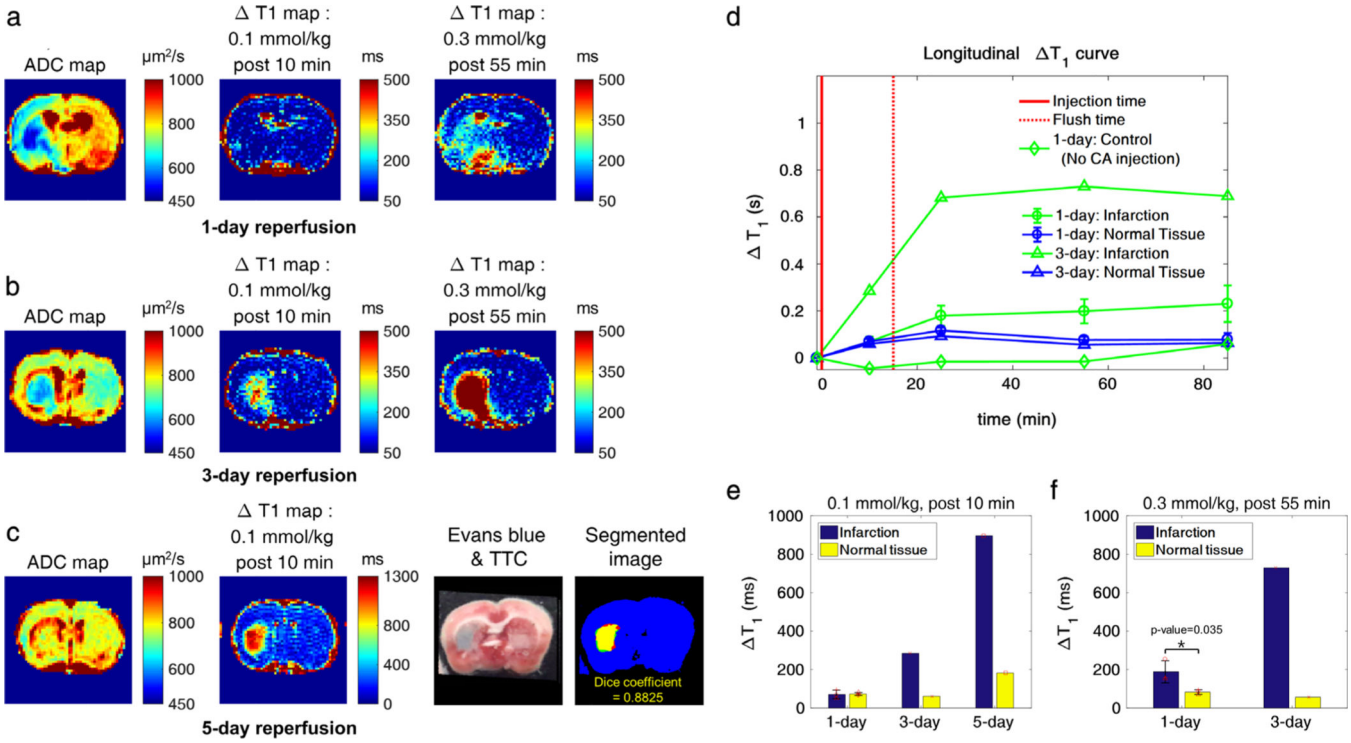

FIGURE 1:

ΔT_1 maps for the MCAO models. **a,b:** ADC and ΔT_1 maps at injection doses of 0.1 mmol/kg (post-10 min) and 0.3 mmol/kg (cumulative, post-55 min) for a 1-day and 3-day reperfusion model, respectively. **c:** The ADC and the ΔT_1 map for a 0.1 mmol/kg CA injection dose post-10 min for a 5-day reperfusion model. Corresponding Evans blue staining results are shown to illustrate the association of elevated region of ΔT_1 maps with respect to the area with BBB damage. Red regions indicate TTC-stained brain tissue. BBB damaged regions from Evans blue (red mask) and ΔT_1 maps (green mask) are respectively shown in the segmented image. The yellow mask represents the overlapping (Dice coefficient = 0.8825) regions between Evans blue and ΔT_1 maps. **d:** Longitudinal ΔT_1 curves up to 85 min postinjection for infarcted and healthy brain regions in a 1-day and 3-day reperfusion model, where the solid red line marks the 0.1 mmol/kg CA injection point and the dotted red line the injection of the additional 0.2 mmol/kg CA flush. The longitudinal ΔT_1 curve of infarction for a non-CA-injected 1-day reperfusion model (negative control) demonstrates the lack of significant ΔT_1 increases, due to ongoing ischemia (d, green diamond line). **e,f:** Corresponding ΔT_1 values for different models (n = 3 for the 1-day mean ± SD, and n = 1 each for the 3-day and 5-day reperfusion model, respectively) for 0.1 mmol/kg (post-10 min) and 0.3 mmol/kg (post-55 min), respectively.

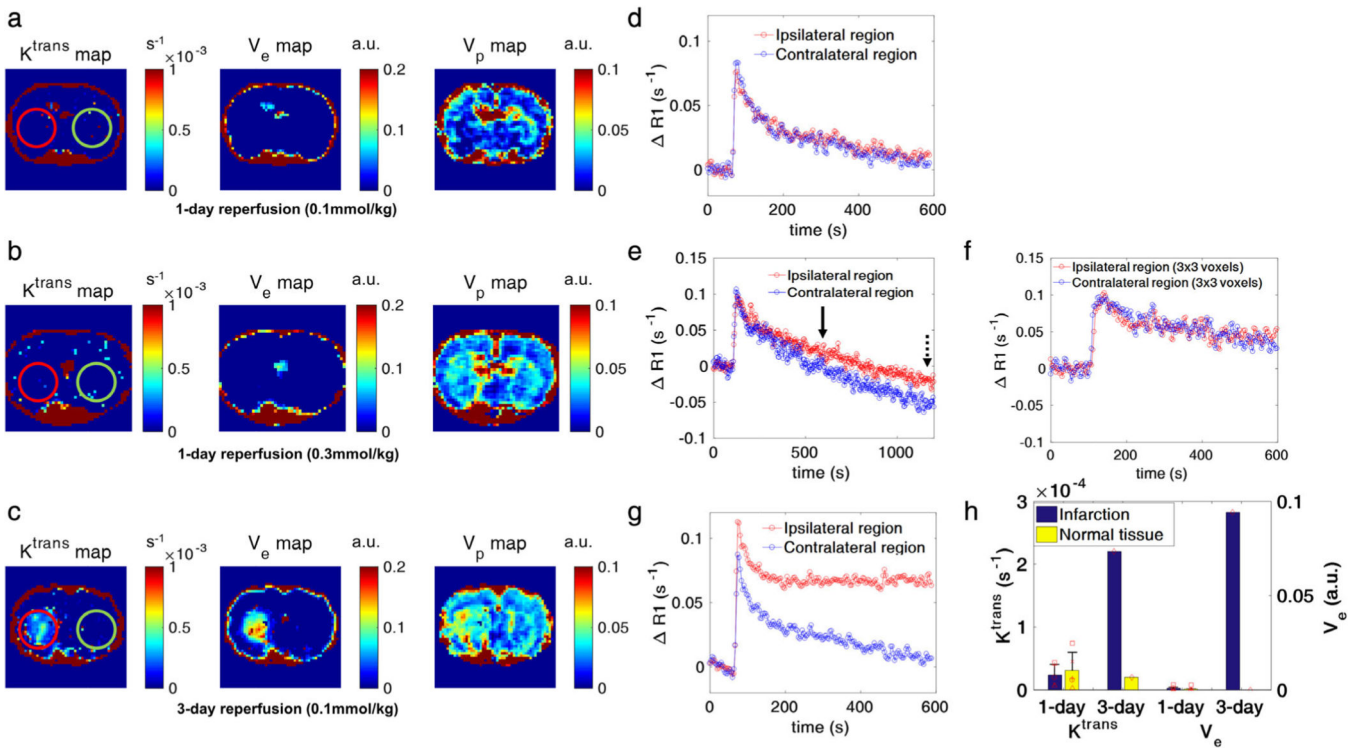

FIGURE 2:

DCE-MRI experimental results for the MCAO models. **a,b:** Permeability (K^{trans}), extracellular extravascular space volume (V_e), and blood volume (V_p) maps from 1-hour MCAO with 24-hour reperfusion models at injection doses of 0.1 mmol/kg and 0.3 mmol/kg, respectively. **c:** Corresponding plots for a 1-hour MCAO with 3-day reperfusion model. **d,e,g:** ROI-based ΔR_1 curves (red line: ipsilateral region, blue line: contralateral region) of the ROIs marked on the K^{trans} maps (red circle: ipsilateral region, green circle: contralateral region) in a–c. The number of voxels in the ROI was ~60 voxels for each case. **f:** Averaged ΔR_1 curve from 3 × 3 voxels in ischemic lesion for comparison with corresponding DSC-MRI time–intensity curve. For the 0.3 mmol/kg dose of ΔR_1 curves (e), 10 min and 20 min after CA injection are marked as solid and dotted line, respectively. **g:** The K^{trans} and V_e values of infarction and contralateral healthy brain for the 1-day ($n = 5$, mean ± SD) and 3-day ($n = 1$) reperfusion models. There was no significant K^{trans} and V_e value differences between normal tissue and infarction with the 1-day reperfusion model ($n = 5$, $P = 0.631/0.583$, unpaired t-test).

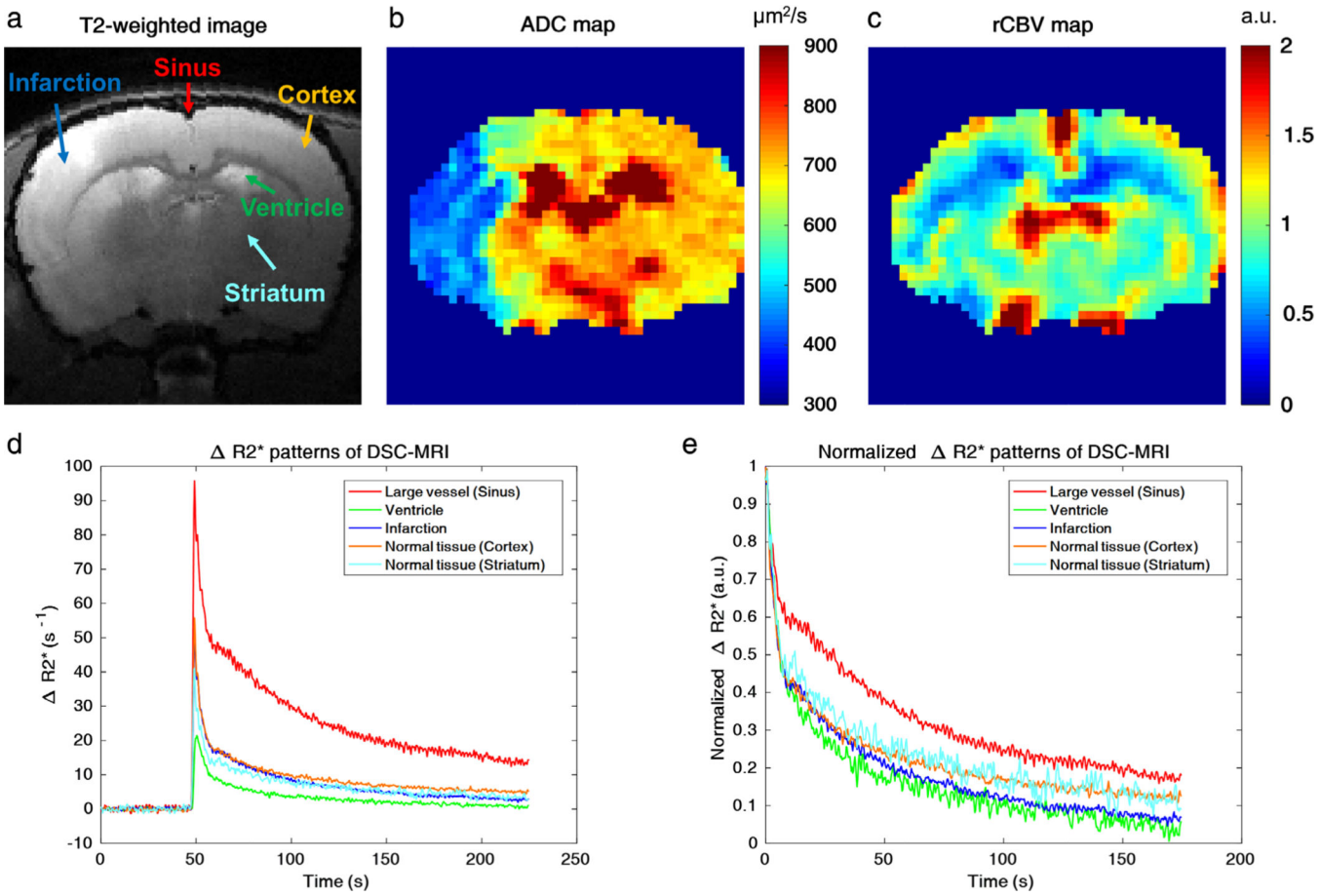

FIGURE 3:

Dynamic ΔR_2* patterns of five different brain regions. **a:** Five different ROIs on a T_2-weighted MR image (red arrow: sinus, green arrow: ventricle, blue arrow: infarction, orange arrow: cortex, cyan blue arrow: striatum). **b,c:** ADC and rCBV maps, respectively. **d,e:** Raw and normalized ΔR_2* time-intensity curves based on the five ROIs from Fig. 3a, respectively (red line: sinus, green line: ventricle, blue line: infarction, orange line: cortex, cyan blue line: striatum). The ROIs have the same voxel size (3 × 3 voxels) and the arrows indicate the center of the respective ROIs.

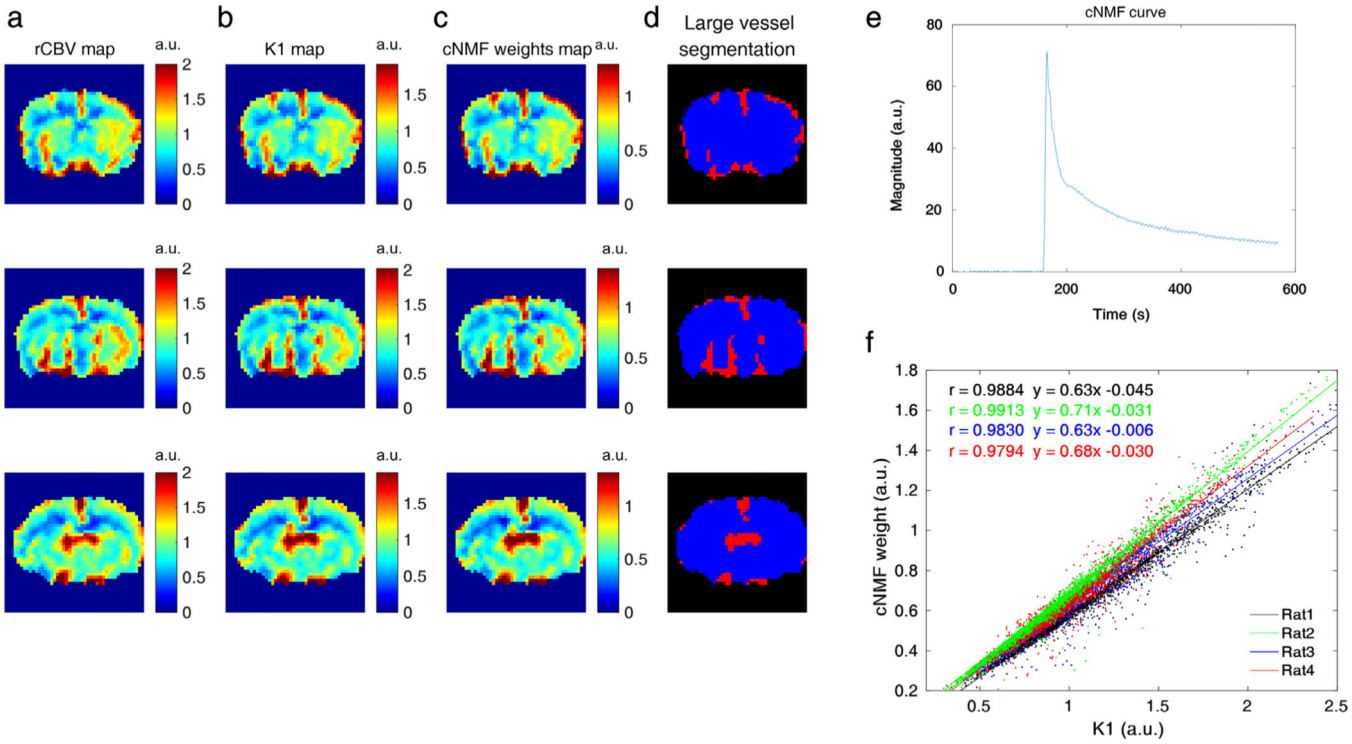

FIGURE 4:

a–c: rCBV, K_1, and cNMF-weight maps with k (the number of patterns) = 1, respectively. **d:** The segmented large vessel regions (red = large vessels). Each row of a–d corresponds to different adjacent slices of a representative rat (rat2) brain scan. **e:** A representative cNMF curve with $k = 1$. **f:** Scatterplots between cNMF weights and K_1 values for four different rats (dot: data, line: correlation curve, black: rat1, green: rat2, blue: rat3, red: rat4).

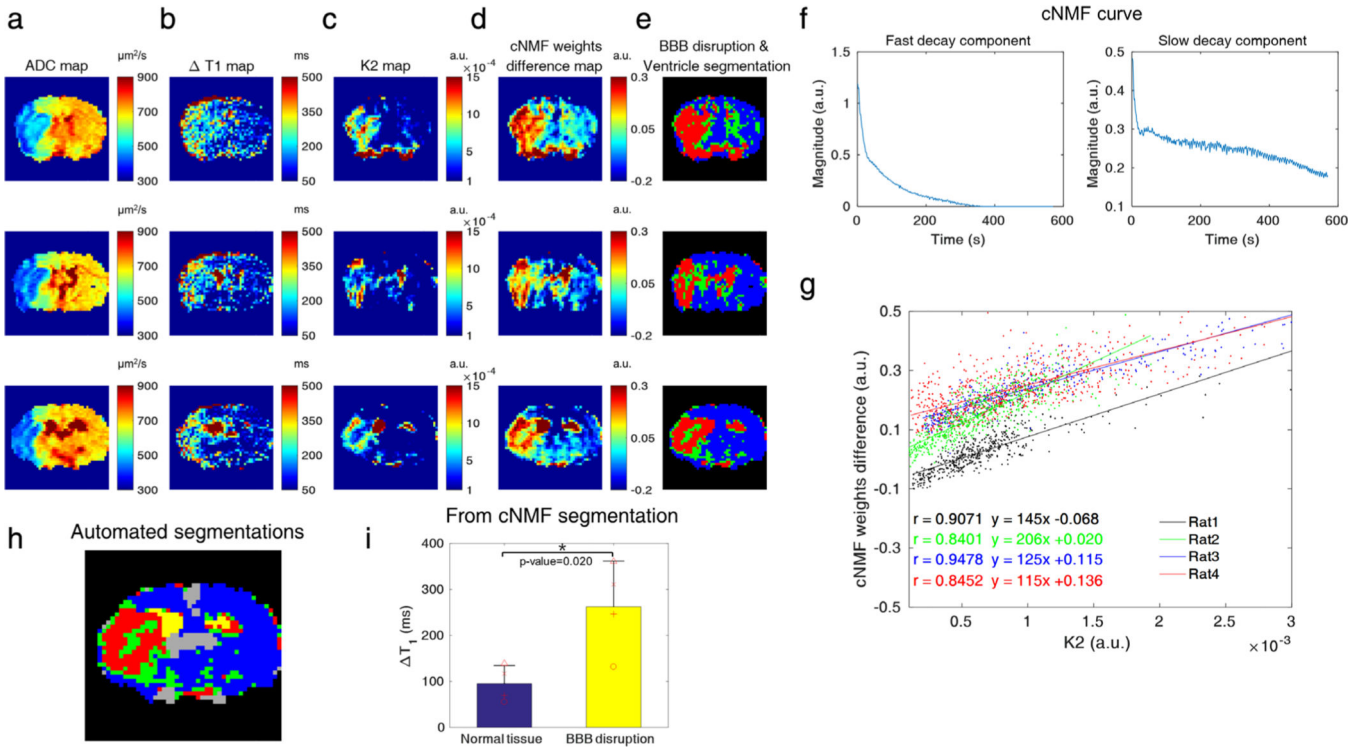

FIGURE 5:

a–d: The ADC map, ΔT_1 map, K_2 map, and cNMF-weights difference map with k (the number of patterns) = 2, respectively. **e:** The segmentation results to identify the BBB-damaged and ventricle regions (red: ventricle and BBB-damaged regions, green: a mixture of healthy and BBB-damaged brain, blue region: healthy brain). Each row of a–e corresponds to different adjacent slices of the same rat (rat2) and slices as displayed in Fig. 4a–d. **f:** Representative cNMF curves with $k = 2$ (left figure: fast decay component, right figure: slow decay component). **g:** Scatterplots between cNMF weight and K_2 for four different rats (dot: data, line: correlation curve, black: rat1, green: rat2, blue: rat3, red: rat4). The ipsilateral regions that had larger K_2 values (manual ROI-derived K_2) than 10^{-4} were used for the scatterplots to relate K_2 and cNMF weights. **h:** cNMF segmentations of five areas (yellow: ventricle, red: BBB-damaged regions, green: a mixture of healthy and BBB-damaged brain, blue: healthy brain, gray: large vessels). **i:** The values of ΔT_1 from cNMF classified BBB-damaged regions (red) and corresponding normal tissue, indicating the association of BBB-damage with DSC-MRI-derived leakage index (K_2). There was a significant ΔT_1 difference between healthy brain tissue and BBB-damaged regions, as derived from the cNMF segmentation ($n = 4$, mean ± SD, $P = 0.020$, unpaired t-test).

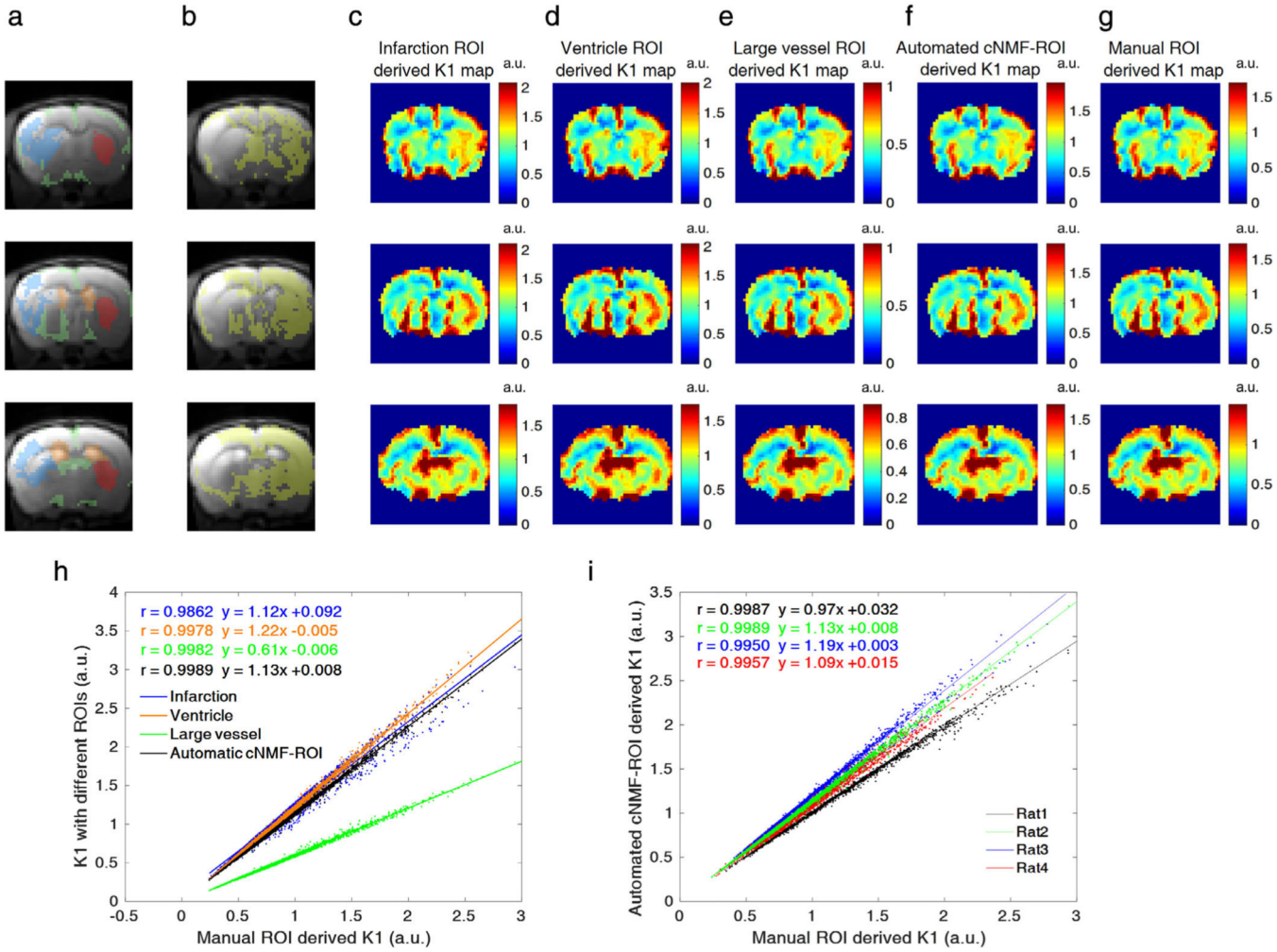

FIGURE 6:

a,b: Five different ROIs (blue: BBB-damaged regions, orange: ventricles, green: large vessels, red: manual ROI, yellow: automated cNMF-ROI). **c–g:** Corresponding K_1 maps from five different ROIs, when a respective ROI was chosen as an intact BBB region. Each row of a–g corresponds to different slices of a representative rat (rat2) brain scan. **h:** Scatterplots between K_1 values derived from four different ROIs and reference (manual) ROIs (dot: data, line: correlation curve, blue: BBB-damaged, orange: ventricle, green: vessel, black: automated cNMF-ROI) for a representative rat (rat2) averaged for all slices. **i:** Scatterplots between K_1 values derived from four automated cNMF-ROIs and reference (manual) ROIs for four different rats (dot: data, line: correlation curve, black: rat1, green: rat2, blue: rat3, red: rat4).

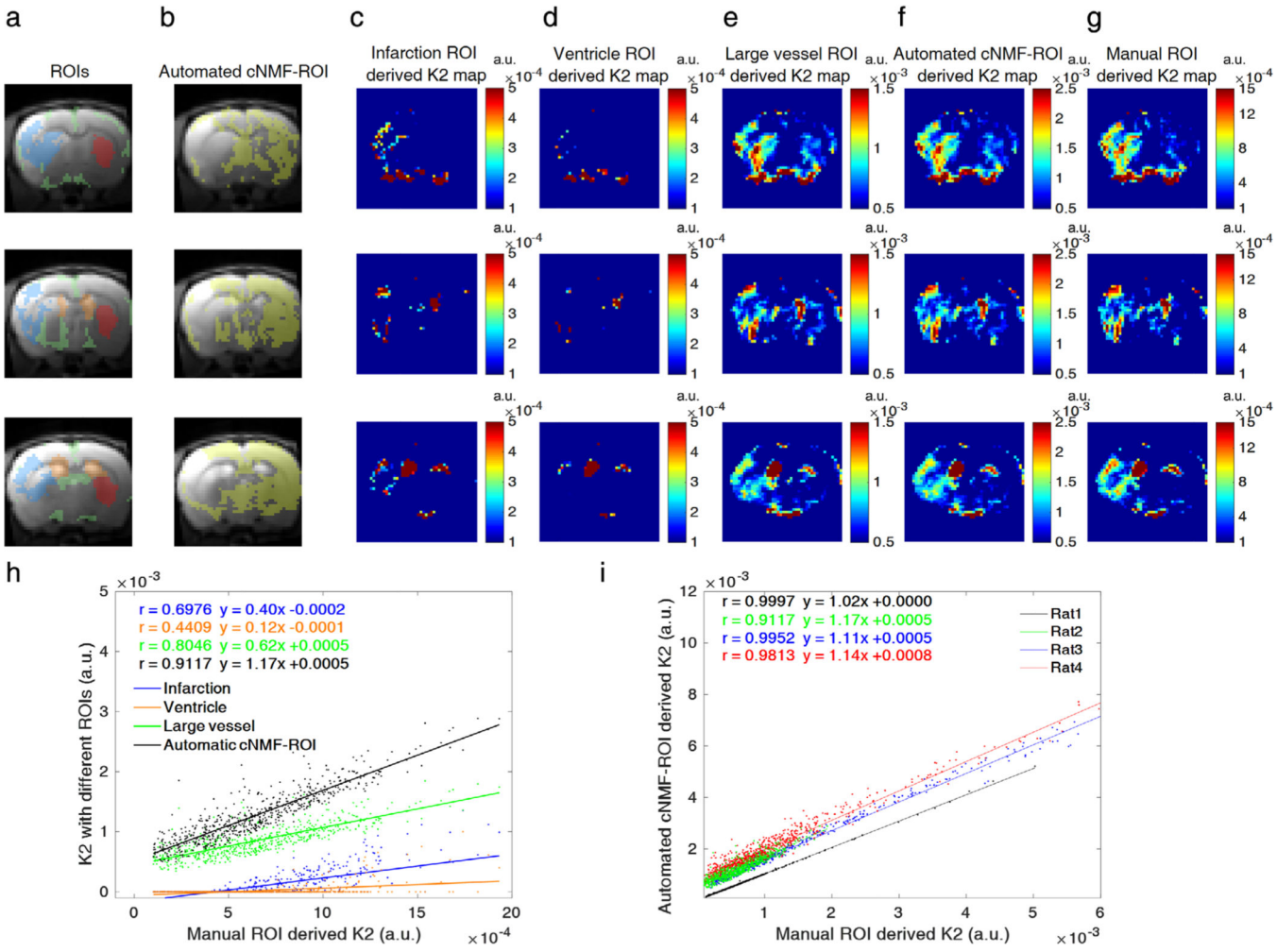

FIGURE 7:

a,b: Five different ROIs (blue: BBB-damaged region, orange: ventricles, green: large vessels, red: manual ROI, yellow: automated cNMF-ROI). **c–g:** Corresponding K_2 maps from five different ROIs, when denoted ROI is chosen as an intact BBB region. Each row of a–g corresponds to different slices of a representative rat (rat2) brain scan. **h:** Scatterplots between K_2 values derived from four different ROIs and reference (manual) ROIs (dot: data, line: correlation curve, blue: infarction, orange: ventricle, green: vessel, black: automated cNMF-ROI) for a representative rat (rat2) averaged for all slices. **i:** Scatterplots between K_2 values derived from four automated cNMF-ROIs and reference (manual) ROIs for four different rats (dot: data, line: correlation curve, black: rat1, green: rat2, blue: rat3, red: rat4). The ipsilateral regions that had larger K_2 values (manual ROI-derived K_2) than 10^{-4} were used for the scatterplots to relate manual ROI-derived K_2 and cNMF ROI-derived K_2.

TABLE 1.

Summarized experimental parameters for each tMCAO group

Occlusion/reperfusion times of MCAO model	MRI acquisitions	Number of animals (comments)
1h-MCAO/1-day reperfusion	DCE-MRI (0 mmol/kg), ΔT_1 map	$n = 1$ (control study without contrast agent injection)
1h-MCAO/1-day reperfusion	DCE- MRI (0.1 mmol/kg), ΔT_1 map	$n = 3$
1h-MCAO/1-day reperfusion	DCE- MRI (0.3 mmol/kg), ΔT_1 map	$n = 2$
1h-MCAO/1-day reperfusion	DSC- MRI (0.3 mmol/kg), ΔT_1 map	$n = 4$
1h-MCAO/3-day reperfusion	DCE- MRI (0.1 mmol/kg), ΔT_1 map	$n = 1$ (control case for conspicuous BBB-leakage)
1h-MCAO/5-day reperfusion	ΔT_1 map	$n = 1$ (Evans blue matching)